Journal of Biomechanics 95 (2019) 109326

Contents lists available at ScienceDirect

Journal of Biomechanics

journal homepage: www.elsevier.com/locate/jbiomech
www.JBiomech.com

Age-related properties at the microscale affect crack propagation in cortical bone

Anna Gustafsson [a,*], Mathias Wallin [b], Hanna Isaksson [a]

[a] Department of Biomedical Engineering, Lund University, Box 118, SE-221 00 Lund, Sweden
[b] Division of Solid Mechanics, Lund University, Box 118, SE-221 00 Lund, Sweden

ARTICLE INFO

Article history:
Accepted 25 August 2019

Keywords:
Porosity
Fracture energy
Tensile test
XFEM
Microstructure

ABSTRACT

The increased risk for fracture with age is associated not only with reduced bone mass but also with impaired bone quality. At the microscale, bone quality is related to porosity, microstructural organization, accumulated microdamage and intrinsic material properties. However, the link between these characteristics and fracture behavior is still missing. Bone tissue has a complex structure and as age-related compositional and structural changes occur at all hierarchical length scales it is difficult to experimentally identify and discriminate the effect of each mechanism. The aim of this study was therefore to use computational models to analyze how microscale characteristics in terms of porosity, intrinsic toughness properties and microstructural organization affect the mechanical behavior of cortical bone. Tensile tests were simulated using realistic microstructural geometries based on microscopy images of human cortical bone. Crack propagation was modelled using the extended finite element method where cement lines surrounding osteons were modelled with an interface damage law to capture crack deflections along osteon boundaries. Both increased porosity and impaired material integrity resulted in straighter crack paths with cracks penetrating osteons, similar to what is seen experimentally for old cortical bone. However, only the latter predicted a more brittle failure behavior. Furthermore, the local porosity influenced the crack path more than the macroscopic porosity. In conclusion, age-related changes in cortical bone affect the crack path and the mechanical response. However, increased porosity alone was not driving damage in old bone, but instead impaired tissue integrity was required to capture brittle failure in aging bone.

1. Introduction

Aging increases the risk for fracture (Burr, 2019; Hui et al., 1988; Melton, 1990), but clinical tools based on bone mineral density measurements currently used for osteoporosis diagnostics are insufficient for predicting fracture risk (Kanis et al., 2019; McCreadie and Goldstein, 2000). This is because bone's ability to resist fracture is not determined only by bone mass but also by the quality throughout the hierarchical structural levels of bone (Boskey and Imbert, 2017; Hernandez and Keaveny, 2006; Ritchie, 2010). The quality of cortical bone at the microscale is largely related to the porosity, microstructural organization, accumulated microdamage and intrinsic material properties, which depend on structure, composition and cellular activity at the lower length scales (Burr, 2004). However, the link between the microscale characteristics and fracture behavior and fracture risk is still missing.

Many microstructural features in cortical bone change with age, e.g., aging is associated with increased porosity (Cooper et al., 2007; Feik et al., 1997; Malo et al., 2013; Mirzaali et al., 2016; Nirody et al., 2015; Stein et al., 1999; Zimmermann et al., 2016), increased number of pores (Nirody et al., 2015), increased pore size (Nirody et al., 2015), increased interconnected pore spaces (Granke et al., 2016; Tong et al., 2015), and decreased area fraction of osteonal tissue (Britz et al., 2009; Granke et al., 2016). Aging also leads to an increase in accumulated microdamage in the form of linear microcracks in the tissue (Agnew et al., 2017; Diab and Vashishth, 2007; Zioupos, 2001). Many of these changes can be explained by age-related alterations in the bone remodeling process, which results in an imbalance between bone formation and bone resorption (Seref-Ferlengez et al., 2015). Mechanical properties also change with age, and while local tissue stiffness seems to be more related to the age of the tissue, i.e. interstitial vs remodeled osteonal tissue, than the age of the person (Mirzaali et al.,

* Corresponding author.
E-mail addresses: anna.gustafsson@bme.lth.se (A. Gustafsson), mathias.wallin@solid.lth.se (M. Wallin), hanna.isaksson@bme.lth.se (H. Isaksson).

https://doi.org/10.1016/j.jbiomech.2019.109326
0021-9290/

2016; Rho et al., 2002), the fracture toughness of cortical bone is inversely correlated to the age of the person (Granke et al., 2016; Koester et al., 2011; Nalla et al., 2004). Young, healthy bone is tough, requiring an increasing amount of energy to propagate a crack through the tissue. The high toughness is attributed to multiple toughening mechanisms that arise when the propagating crack interacts with the microstructure, causing deflections along osteon boundaries, twists and bridges (Koester et al., 2008; Ritchie, 2010; Zimmermann et al., 2009). This behavior is at the macroscale manifested as increasing crack resistance in the R-curves. In contrast, old bone seems to have lost many of these toughening mechanisms and instead display largely straight crack paths that penetrate osteons, and exhibits flat R-curves (Chan et al., 2009; Katsamenis et al., 2015; Koester et al., 2011; Nalla et al., 2006; Nalla et al., 2004).

As bone tissue is complex and alterations due to aging can take place at all hierarchical length scales simultaneously it is difficult to experimentally discriminate the effect of the different mechanisms. An alternative is to use computational models and a handful of studies have used the extended finite element method (XFEM) to simulate crack propagation in cortical bone at the microscale. However, the majority of these studies did not predict realistic crack paths as they could not capture crack deflections at osteon boundaries (Abdel-Wahab et al., 2012; Idkaidek and Jasiuk, 2017; Li et al., 2013; Vergani et al., 2014). To capture crack deflections, Marco et al. (2018a) proposed a maximum tangential stress criterion where all possible crack paths in front of the crack tip were scanned to find the weakest path. We have adopted a different approach and used an interface damage law, inspired by cohesive element models (Mischinski and Ural, 2011), to model damage in the cement lines (Gustafsson et al., 2019a). We have previously shown using idealized geometries that this framework can capture crack deflections at osteon boundaries (Gustafsson et al., 2019a; Gustafsson et al., 2019b). In the current study we instead used realistic microstructural geometries based on microscopy images of human cortical bone. The aim of the study was to analyze how microscale characteristics in terms of porosity, intrinsic toughness properties and microstructural organization affect the mechanical behavior of cortical bone. The hypothesis was that age-related alterations in cortical bone tissue would affect the crack path and embrittle the material making it more susceptible to fracture. The main question is: *What drives damage in old compared to young cortical bone - increased porosity or impaired material integrity?*

2. Methods

2.1. Cortical bone interface damage model

Realistic cortical bone geometries including osteons embedded in an interstitial matrix and surrounded by cement lines were created based on a scanning acoustic microscopy (SAM) image from the tibial shaft (Fig. 1A, male donor, 70 years of age with no reported diseases). Please see the study by Iori et al. (2019) for details. A subregion of 1×1 mm^2 was selected (Fig. 1B) and osteons and Haversian canals were segmented manually using SEG3D (Fig. 1C, SEG3D version 2.4, CIBC, University of Utah). Ellipses were fitted to all segmented osteons and canals using an in-house Matlab code (Fig. 1D, Matlab version 2018b, The MathWorks, Inc., Natick, Massachusetts). Two-dimensional (2D) finite element models were created in Abaqus (Fig. 1E, Abaqus v2017, Dassault Systemes SIMULIA, Johnston, RI) and a python script was used to import the geometrical parameters describing the microstructure (Fig. 1F) together with the coordinates of the centroid and the angle of rotation. The matrix domain was expanded to 1.2×1.2 mm^2 to avoid cutting the osteons at the model boundaries (Fig. 1E). Cement line interfaces (red ellipses in Fig. 1) were created around all osteons with a thickness of 5 μm and normal vectors $\boldsymbol{n}$ were defined for all points along the cement lines (see details below). Four material phases, representing interstitial matrix, osteons, cement lines and Haversian canals were modelled as linear isotropic elastic materials with material parameters according to Table 1 (Gustafsson et al., 2019a; Gustafsson et al., 2019b). Tensile tests until failure were simulated using displacement-controlled loading in a quasi-static analysis (Fig. 1G).

The extended finite element method (XFEM) with the cohesive segments approach was used to model crack propagation in the cortical bone models using our previously presented framework (Gustafsson et al., 2019a; Gustafsson et al., 2019b). The maximum principal strain criteria (MAXPE) was used to model crack propagation in matrix, osteon and Haversian canals. For the cement line interface, a user-defined damage initiation criterion, including both the MAXPE criteria and the quadratic nominal strain criteria (QUADE) was used, where the crack direction in the QUADE criteria was defined by vectors $\boldsymbol{n}$ oriented perpendicular to the cement line interface (Fig. 1F). The normal vectors, $\boldsymbol{n}$, in all cement line elements were defined (Fig. 1E) from the gradient of

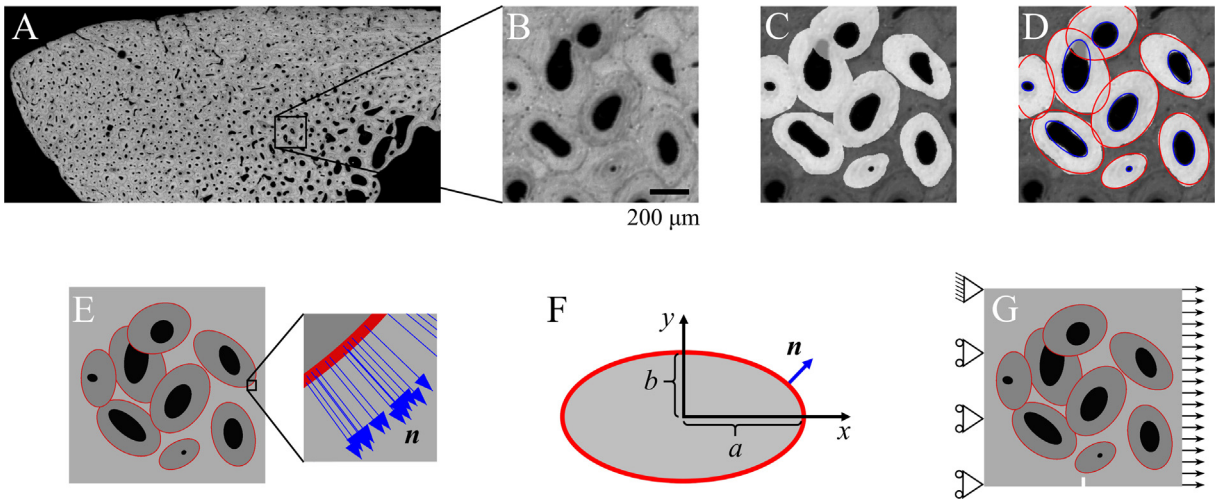

Fig. 1. Pipeline illustrating the model development. (A) SAM image of human cortical bone where (B) a sub-section of 1×1 mm^2 was selected. (C) Osteons (white) and canals (black) were segmented manually. (D) Ellipses were fitted to all canals and osteons and used to define the microstructural FE-geometries. (E) Normal vectors were assigned to all cement line elements and (F) defined for all points along the ellipses. (G) Boundary conditions for tensile tests with an initial crack inserted in the lower edge.

Table 1
Material parameters. Young's modulus, Poisson's ratio, critical damage initiation strain for the MAXPE criterion, critical interface damage initiation strain for the QUADE criterion and strain energy release rate specified for interstitial matrix, osteon, Haversian canals and cement lines.

	Matrix	Osteon	Cement line	Canal
E (MPa)	15 000	12 000	18 000	10
ν	0.3	0.3	0.3	0.3
ε^0_{max}	0.004	0.004	0.004	0.004
ε^0_{cl}	–	–	0.0015	–
G (kJ/m^2)	0.4	0.4	0.4	0.000001

$$f(x,y) = \frac{x^2}{a^2} + \frac{y^2}{b^2} - 1 = 0$$

i.e.

$$\nabla f = \left(\frac{2x}{a^2}, \frac{2y}{b^2}\right)$$

The damage evolution inside the cohesive crack was assumed to be mode-independent for all damage criteria and materials and was modelled with an energy-based evolution law with a linear softening behavior. The fracture energy G (also referred to as the strain energy release rate) was used to specify the amount of energy needed to create a fully open cohesive crack. For a more detailed description of the damage models used to simulate crack propagation, please refer to our previous studies (Gustafsson et al., 2019a; Gustafsson et al., 2019b).

2.2. Simulations

2.2.1. Effect of porosity

To test the effect of porosity, five different microstructures were generated (Fig. 2A) based on the SAM-model in Fig. 1. The original 8-osteon model had 9% porosity and additional models with 2%, 7% and 15% porosity were created by changing the size of the ellipses that defined the Haversian canals while preserving the shape, i.e. $\frac{a}{b}$ was constant. These values span over the average cortical porosity reported in literature (e.g., 4%–9% in femoral shaft of women between 20 and 100 years with no known bone diseases (Feik et al., 1997), 8%–16% in femoral shaft of men between 20 and 80 years with no known bone diseases (Malo et al., 2013)). Furthermore, a model with 0% porosity was created by filling all canal areas with osteon material. Plane strain 4-node bilinear elements with reduced integration (CPE4R) were used with a thickness of 1 mm. The maximum element size was 10 μm. Cement line interfaces were meshed with at least two elements across the interface width and the total number of elements was approximately 80 000 for all models (please see the supplementary material in (Gustafsson et al., 2019a) for mesh sensitivity analyses).

2.2.2. Effect of fracture energy

To investigate the effect of the material integrity, the fracture energies for matrix, osteon and cement line materials were reduced to 0.2, 0.1 and 0.05 kJ/m^2 and compared to the initial value of 0.4 kJ/m^2. This range covers values for damage initiation reported for young and old bone (Chan et al., 2009; Koester et al., 2008; Nalla et al., 2005; Norman et al., 1995; Zimmermann et al., 2009). The 8-osteon model with 9% porosity was used in all simulations (Fig. 2A).

2.2.3. Effect of osteon distribution

Finally, models with different osteon distributions were analyzed. Two additional subregions from Fig. 1A were selected, both with 7% porosity: one 4-osteon model (Fig. 2B) and one 15-osteon model (Fig. 2C), and compared to the 8-osteon model with 7% porosity (Fig. 2A). Material parameters in Table 1 were used for all geometries.

3. Results

The cortical bone microstructure clearly affected the crack trajectory through two competing mechanisms where cement lines deflected cracks and Haversian canals attracted them (Fig. 3). Due to the attraction from the canals, crack paths were longer in models with intermediate porosities (Fig. 3C-D) compared to models with low porosities (Fig. 3A-B). However, at high porosity, the crack instead penetrated the cement line interfaces and propagated through the osteons (Fig. 3E), which resulted in a straighter crack path. The porosity levels were also reflected in the force-displacement curves (Fig. 3F), where increased porosity rendered lower structural stiffness as well as lowered peak force along with an increased ability to absorb energy before failure (Table 2). The load in models with low porosity increased linearly until the peak load was reached followed by an almost linear decay during crack opening. Porous models displayed a ductile response, followed by a sudden drop in load bearing capacity (Fig. 3F). Crack initiation vs applied deformation was comparable for all models, however, the crack growth rate was negatively correlated to porosity (Fig. 3G).

The fracture energy also affected the crack path (Fig. 4, where Fig. 4A corresponds to Fig. 3D). In models with high fracture energy, the crack deflected along the cement line and propagated around the osteons (Fig. 4A-B). For the lowest fracture energy,

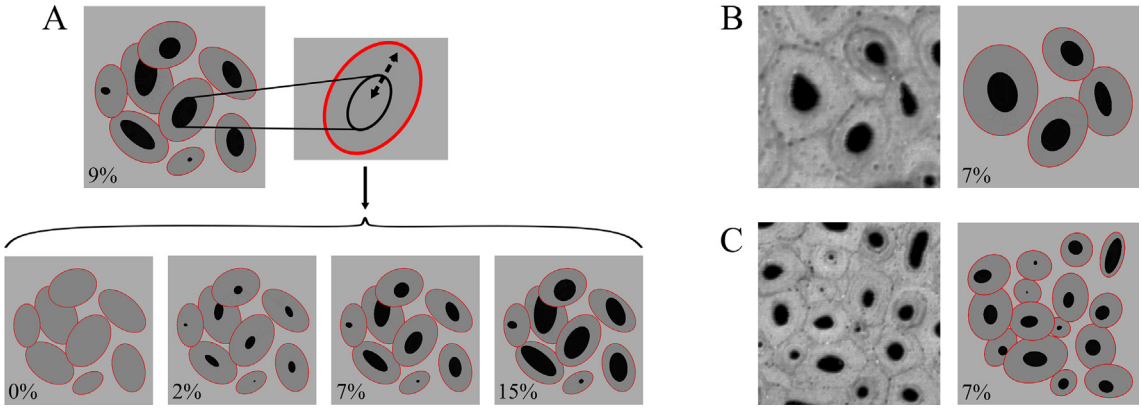

Fig. 2. (A) Five different 8-osteon models with rescaled canals to cover porosities from 0 to 15%. Two additional microstructures with 7% porosity were analyzed: (B) a 4-osteon model and (C) a 15-osteon model.

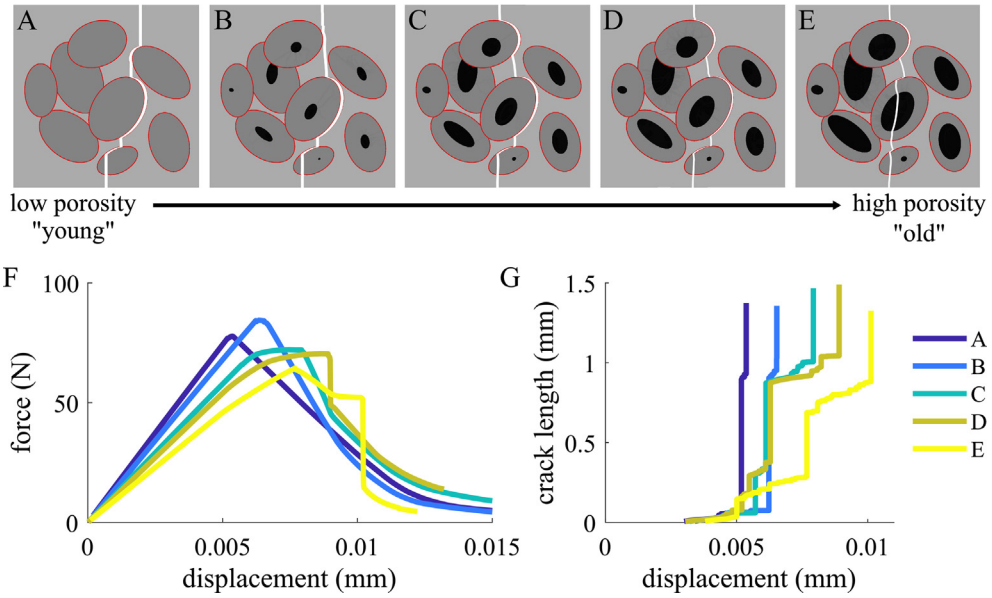

Fig. 3. Influence of porosity on the mechanical response. Models with (A) 0%, (B) 2% (C) 7%, (D) 9% and (E) 15% porosity were evaluated. (F) Force-displacement curves and (G) crack growth curves corresponding to the microstructures in (A)–(E).

Table 2
Quantitative results in terms of crack length, stiffness, work to fracture and peak force. The stiffness was calculated as the slope of a line fitted to all data points between 0 and 50 N in the force-displacement curve and the work to fracture is the area under the force-displacement curve until the force dropped to 10 N.

Input				Results			
Model		Porosity (%)	Fracture energy (kJ/mm^2)	Crack length (mm)	Stiffness (kN/mm)	Work to fracture (Nmm)	Peak force (N)
Porosity (Fig. 3)	8-ost	0	0.4	1.37	14.9	0.503	78
		2	0.4	1.36	13.6	0.501	84
		7	0.4	1.47	11.6	0.529	72
		9	0.4	1.49	10.8	0.513	70
		15	0.4	1.33	9.1	0.412	64
Material integrity (Fig. 4)	8-ost	9	0.4	1.49	10.8	0.513	70
		9	0.2	1.50	10.8	0.316	60
		9	0.1	1.33	10.8	0.177	54
		9	0.05	1.23	10.8	0.115	50
Microstructure (Fig. 5)	4-ost	7	0.4	1.32	11.6	0.432	65
	8-ost	7	0.4	1.47	11.6	0.529	72
	15-ost	7	0.4	1.39	11.8	0.528	78

the crack instead penetrated the cement line and propagated through the osteons (Fig. 4D). With a fracture energy of 0.1 kJ/m^2 (Fig. 4C), the crack propagated through the first osteons and deflected around the last osteon, making this crack path a combination of the predicted crack paths for high and low fracture energies. The effect of the fracture energy was also clearly visible in the force-displacement curve (Fig. 4E), where models with low fracture energy displayed a brittle behavior and models with high fracture energy showed a ductile response. This behavior was also reflected in the crack growth rate (Fig. 4F), where there was a rapid crack growth after crack initiation in model D with low fracture energy and slower crack growths in models A-C when cracks deflected in the cement lines. A quantitative comparison is presented in Table 2.

The stiffness was virtually the same for all models with equal porosity at 7% although they had different osteon distributions (Fig. 5D and Table 2). The peak force was however lower for the 4-osteon model and higher for the 15-osteon model compared to the model with 8 osteons. The crack paths followed the trends seen previously in Fig. 3, where the crack propagated through an osteon with a large canal, as seen in the 4-osteon model (Fig. 5A) and deflected in cement lines surrounding osteons with smaller canals (Fig. 5A-C). Again, the rate of the crack growth was lowered when the propagating crack interacted with the microstructure (Fig. 5E).

4. Discussion

The fracture risk increases with age and the underlying mechanisms are believed to be related to structural and compositional changes in the tissue (Burr, 2019). However, to understand the differences in damage evolution in old compared to young bone it is necessary to evaluate the contributions of different age-related factors. In this study, the effect of porosity and intrinsic fracture toughness was analyzed for different cortical bone geometries based on microscopy images of human bone. Both factors affected the crack propagation and increased porosity and reduced fracture energy resulted in straighter crack patterns with cracks propagating through osteons instead of deflecting along the cement lines. These results agree with crack patterns found for old bone (Chan et al., 2009). However, alterations in porosity and fracture energy had different effects on the mechanical behavior of the simulated bone tissue, where porous models displayed a ductile behavior with large deformations at failure while models with low fracture

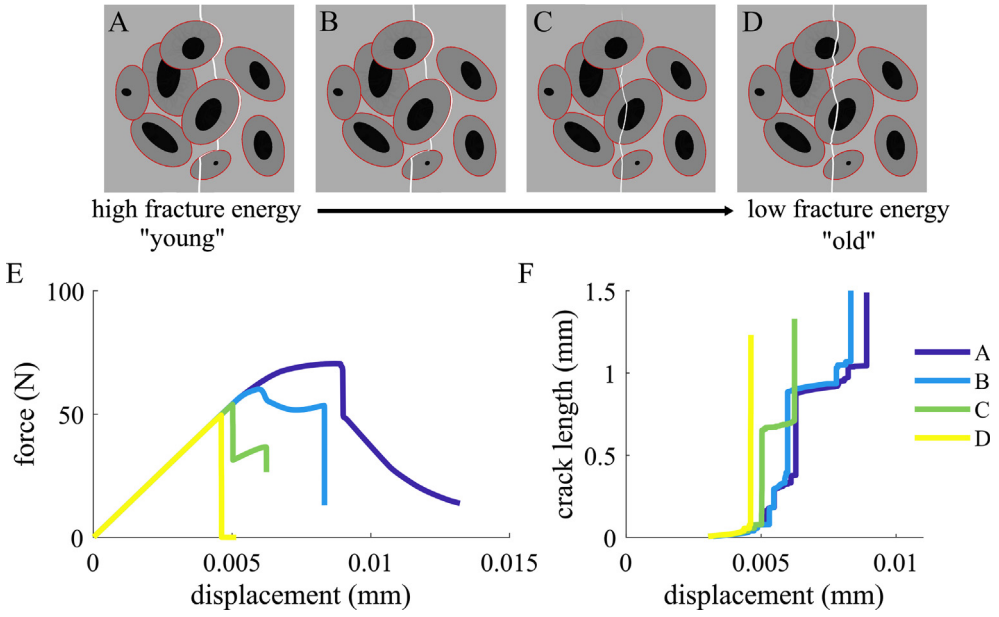

Fig. 4. Influence of fracture energy on the mechanical response (9% porosity). The fracture energies (A) 0.4 kJ/m^2, (B) 0.2 kJ/m^2, (C) 0.1 kJ/m^2 and (D) 0.05 kJ/m^2 were evaluated. (E) Force-displacement curves and (F) crack growth curves corresponding to the microstructures in (A)–(D).

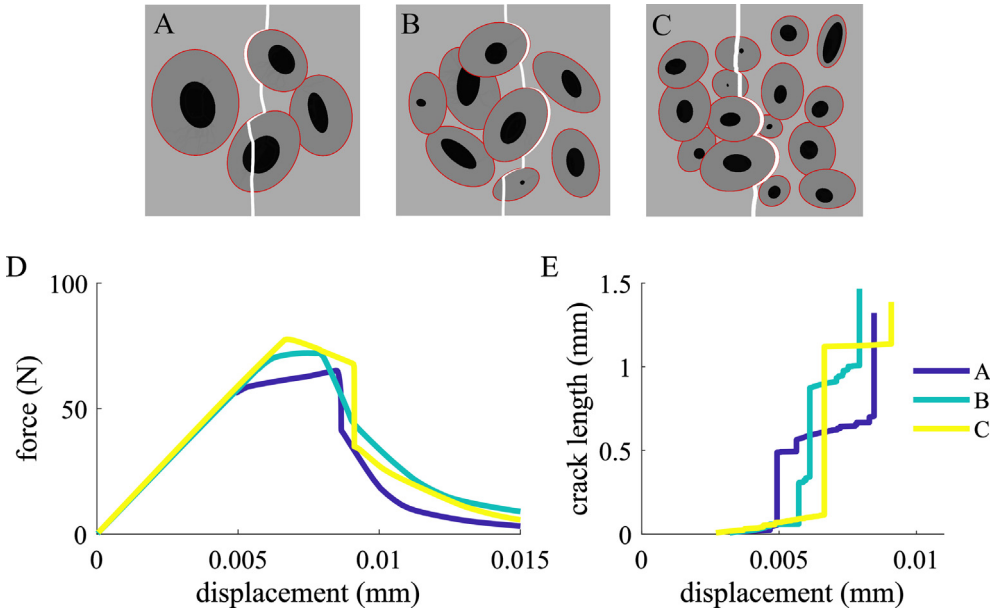

Fig. 5. (A–C) Crack paths in models with different microstructure and 7% porosity. (D) Force-displacement curves and (E) crack growth curves corresponding to the microstructures in (A)–(C).

energy failed in a brittle way. This is different from what has been reported from experimental studies, where high porosity has been correlated to brittle failure (Chan et al., 2009). The modelling results suggest that porosity alone is not driving damage in old bone and support the idea that alterations in the tissue matrix affecting the intrinsic toughness properties are important for the increased fracture risk with age (Burr, 2019; Unal et al., 2018).

The fracture energy that describes the degradation of the cohesive crack had a large influence on both the mechanical behavior of the bone samples and on the crack trajectories. The crack pattern was gradually changed when reducing the facture energy of the tissue, from crack deflection at osteon borders at high energies to crack propagation through osteons at low energies. In this study, equal fracture energies were assumed for both matrix, osteons and cement lines, as distinct values are not possible to measure experimentally. This assumption was shown to have a small effect on the crack pattern and peak force in our previous parameter study (Gustafsson et al., 2019b). The tested fracture energies from 0.05 to 0.4 kJ/mm^2 span experimental values for crack initiation in old and young cortical bone (Chan et al., 2009; Koester et al., 2008; Nalla et al., 2005; Norman et al., 1995; Zimmermann et al., 2009) and the trends in the predicted crack patterns are similar to those reported in fracture tests (Chan et al., 2009). In total, three different crack paths were predicted, where the crack paths for the two higher fracture energies coincided and the crack path was gradually straighter for the two lower energies. All four models had very

distinct load curves (Fig. 4E) ranging from ductile to very brittle failure behavior. Worth noticing is that the load bearing capacity in Fig. 4C was recovered when the crack deflected around the last osteon.

All three models with different microstructures and constant 7% macroscopic porosity resulted in equal initial stiffness. Nevertheless, both the peak force and the crack paths were influenced by the local porosity, i.e. pores close to the fracture line (Table 2). In the 4-osteon model with large pores (Fig. 5A), the crack propagated through the large osteon similar to the high porosity model in Fig. 3E. Based on literature, it is not clear how the osteon distribution (e.g. number, size, area fraction etc.) change with age (Britz et al., 2009; Granke et al., 2016; Nirody et al., 2015; Tong et al., 2015), and the contradictory findings makes it difficult to directly compare the geometries in Fig. 5 to the aging process in cortical bone. Still, the concept that the local pore distribution rather than the macroscopic porosity is important for crack propagation is highly relevant for aging in cortical bone, where disturbed remodeling drastically can alter the pore distribution. This is also in line with the idea that damage is a local process that should be studied using local techniques (Gustafsson et al., 2018).

Both increased porosity and reduced fracture toughness promoted crack propagation through osteons, suggesting that both factors are relevant alterations in old bone, however, only reduced fracture toughness resulted in a brittle behavior. Experimentally it is difficult to discriminate the effect of factors that are changing simultaneously with age, as they might change independently of each other. This ambiguity could be why *age* itself is correlated to fracture toughness (Granke et al., 2016) and fracture risk (Burr, 2019). In the XFEM models, the intrinsic toughness of the tissue was represented by the fracture energy needed to open the cohesive crack and toughening mechanisms taking place at submicron scales, e.g. fiber bridging of the crack or fibrillar sliding, were combined in the cohesive crack description. The intrinsic toughness of bone tissue is related to the organic matrix (Burr, 2019; Unal et al., 2018) and alterations in the collagen phase lead to reduced fracture resistance. Zimmermann et al. (2011) found that increased non-enzymatic collagen crosslinking with age reduced the nanoscale plasticity in cortical bone and Willett et al. (2019) linked reduced fracture toughness to age-related degradation of the collagen network integrity.

The simulations showed that the microstructure influenced the propagating crack using two distinct mechanisms: Haversian canals attracted the crack by altering the surrounding strain field, causing smooth and meandering crack patterns (see e.g. Fig. 4D) and cement line interfaces deflected the cracks causing sharp turns in the crack path (see e.g. Fig. 4A). The crack growth rate was also affected by the microstructure (Fig. 6). Large canals acted as strain

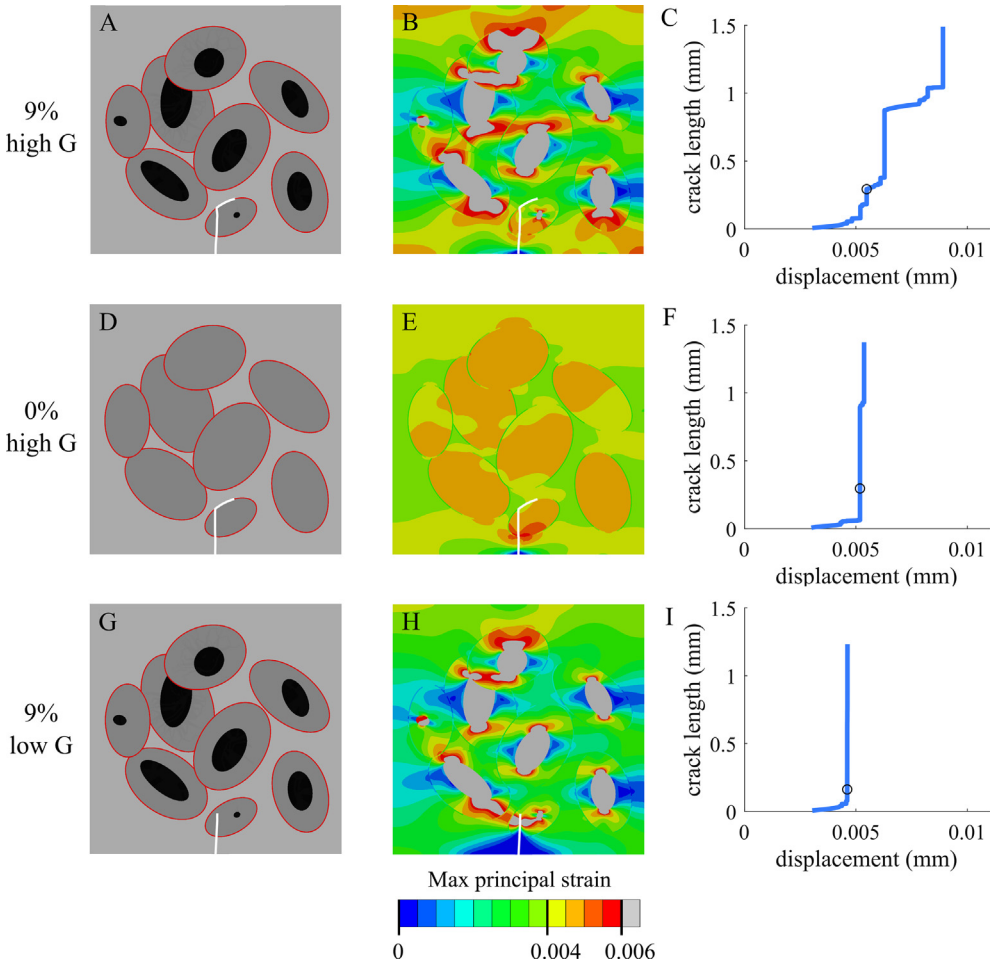

Fig. 6. The influence of the local strain field on the crack growth in the 8-osteon model with varying porosity (top vs middle row) and with varying fracture energy (top vs last row). (A–C): The 8-osteon model with 9% porosity and 0.4 kJ/m^2 fracture energy showed a heterogeneous strain distribution caused by the Haversian canals. At the time point indicated by the black ring in (C), the crack tip was leaving the cement line interface and entering a region with lower strains in the matrix (B), which slowed down the crack growth (C). (D–F): The 8-osteon model without Haversian canals displayed a more homogeneous strain distribution (E) and a more rapid crack growth rate (F). (G–I): The 8-osteon model with 9% porosity and 0.05 kJ/m^2 fracture energy showed high strain localizations around the crack tip that drove the crack through the cement line interfaces (H) and resulted in an almost immediate crack growth after crack initiation (I).

concentrators redistributing the applied deformation, which also resulted in regions with lower strains where the crack growth rate decreased (Fig. 6A-C). In models with no or low porosity, the strain distribution was instead more homogeneous, resulting in a more rapid crack growth (Fig. 6D-F). Moreover, low fracture toughness resulted in high strain concentrations around the crack tip and rapid crack growth with a crack that penetrated cement line interfaces (Fig. 6G-I). Additionally, crack deflection along cement lines also slowed down the subsequent growth in the matrix as the crack tip was redirected into regions with lower strains (Fig. 6A-C). This illustrates the competition between the mechanical crack driving force, in this case the maximum principal strain, and the weak crack paths provided by the microstructure, which was discussed thoroughly by Zimmermann et al. (2009).

Cement lines could not attract cracks in the models, however, the Haversian canal inside the osteon could increase the chance of the crack hitting a cement line (compare e.g. Fig. 3B and C). In cortical bone, however, it is possible that also microdamage in cement lines functions as crack attractors and promotes crack deflection along cement lines (Obrien et al., 2007; Seref-Ferlengez et al., 2015). Wagermaier et al. (2015) reviewed the importance of weak interfaces for bone's resistance to fracture and suggested that lamellar interfaces surrounding Haversian canals protect the tissue by shielding the canals. Hence, canals might not severely weaken the structure, as long as the surrounding interfaces successfully can shield them from approaching cracks. However, in old bone, large resorption cavities that are not surrounded by cement lines or osteonal lamellae can form from imbalanced remodeling. This type of porosity, with large unshielded pores, could therefore be detrimental for bone's resistance to fracture. Granke et al. (2016) found that both porosity and pore clustering had a negative effect on the fracture toughness of cortical bone. Furthermore, the XFEM-models show that the shielding capacity of the cement lines is reduced at low fracture energies (Fig. 4) and consequently the cracks tended to penetrate the cement line and reach the Haversian canals to a larger extent in models with low fracture energy in the matrix. Still, it is possible that other age-related changes in the tissue also affect the capacity to deflect cracks. Kennedy et al. (2008) showed that young osteons were more likely to deflect cracks compared to old osteons and Milovanovic et al. (2018) have shown that the discrepancy in mineralization between osteons and cement lines decrease with age.

In this study, we have shown that our modelling framework can capture realistic crack paths in microstructural models based on human cortical bone. Still, the models have several limitations with simplified linear elastic material descriptions and idealized boundary conditions that could not capture the full complexity of cortical bone. The fact that only one crack was allowed could be one reason for why the effect of porosity was not found as severe for the mechanical behavior of the bone tissue, as new cracks could not initialize even though the damage initiation criteria were fulfilled. Consequently, nor the effect of microdamage occurring away from the crack tip was analyzed. This could potentially be captured by including material plasticity in the models. Furthermore, the tissue microstructure was simplified, assuming homogeneous osteonal and interstitial tissue. Resolving the lamellar structure including the interfaces separating them could give a more nuanced picture of crack propagation in and around osteons by providing more possible crack paths as seen experimentally (see e.g. (Katsamenis et al., 2015)). A further improvement would be to simulate crack propagation in 3D, however, due to limited numerical convergence it is currently not feasible to simulate long or complex crack paths in 3D (Ali et al., 2014; Hammond et al., 2019; Marco et al., 2018b). This limitation was further discussed in previous studies (Gustafsson et al., 2019a; Gustafsson et al., 2019b).

5. Conclusion

Cortical bone is a complex material and knowledge about age-related changes in both tissue structure and composition is key to understand, and subsequently predict, the increased fracture risk with age. In this study we have shown that two age-related properties, i.e. increased porosity and reduced fracture energy, can change the trajectory of a propagating crack from deflecting along cement lines to penetrating osteons. Furthermore, local pore size and distribution seem to affect the crack path more than the macroscopic porosity. Nevertheless, these properties have different impact on the mechanical response, where porous models show large deformations at fracture while low fracture energy results in brittle failure. In conclusion, age-related changes in cortical bone affect the crack path and the mechanical response. However, increased porosity alone was not driving damage in old bone, but instead impaired tissue integrity was required to capture brittle failure in aging bone.

Acknowledgements

This work was supported by the Swedish Foundation for Strategic Research [grant number IB2013-0021]. We would also like to thank Professor Kay Raum, Charité, Berlin, for providing scanning acoustic microscopy images collected within the framework of the TaCo-Sound project, supported by the Deutsche Forschungsgemeinschaft [DFG Ra1380/9-1] and by the Agence Nationale de la Recherche [ANR-14-CE35-0030-01].

Declaration of Competing Interest

The authors declare that no conflict of interests exist.

References

Abdel-Wahab, A.A., Maligno, A.R., Silberschmidt, V.V., 2012. Micro-scale modelling of bovine cortical bone fracture: Analysis of crack propagation and microstructure using X-FEM. Comput. Mater. Sci. 52, 128–135.
Agnew, A.M., Dominguez, V.M., Sciulli, P.W., Stout, S.D., 2017. Variability of in vivo linear microcrack accumulation in the cortex of elderly human ribs. Bone Rep. 6, 60–63.
Ali, A.A., Cristofolini, L., Schileo, E., Hu, H.X., Taddei, F., Kim, R.H., Rullkoetter, P.J., Laz, P.J., 2014. Specimen-specific modeling of hip fracture pattern and repair. J. Biomech. 47, 536–543.
Boskey, A.L., Imbert, L., 2017. Bone quality changes associated with aging and disease: a review. Ann. NY Acad. Sci. 1410, 93–106.
Britz, H.M., Thomas, C.D., Clement, J.G., Cooper, D.M., 2009. The relation of femoral osteon geometry to age, sex, height and weight. Bone 45, 77–83.
Burr, D.B., 2004. Bone quality: understanding what matters. J. Musculoskelet. Neuronal. Interact. 4, 184–186.
Burr, D.B., 2019. Changes in bone matrix properties with aging. Bone 120, 85–93.
Chan, K.S., Chan, C.K., Nicolella, D.P., 2009. Relating crack-tip deformation to mineralization and fracture resistance in human femur cortical bone. Bone 45, 427–434.
Cooper, D.M., Thomas, C.D., Clement, J.G., Turinsky, A.L., Sensen, C.W., Hallgrimsson, B., 2007. Age-dependent change in the 3D structure of cortical porosity at the human femoral midshaft. Bone 40, 957–965.
Diab, T., Vashishth, D., 2007. Morphology, localization and accumulation of in vivo microdamage in human cortical bone. Bone 40, 612–618.
Feik, S.A., Thomas, C.D., Clement, J.G., 1997. Age-related changes in cortical porosity of the midshaft of the human femur. J. Anat. 191 (Pt 3), 407–416.
Granke, M., Makowski, A.J., Uppuganti, S., Nyman, J.S., 2016. Prevalent role of porosity and osteonal area over mineralization heterogeneity in the fracture toughness of human cortical bone. J. Biomech. 49, 2748–2755.
Gustafsson, A., Khayyeri, H., Wallin, M., Isaksson, H., 2019a. An interface damage model that captures crack propagation at the microscale in cortical bone using XFEM. J. Mech. Behav. Biomed. Mater. 90, 556–565.
Gustafsson, A., Mathavan, N., Turunen, M.J., Engqvist, J., Khayyeri, H., Hall, S.A., Isaksson, H., 2018. Linking multiscale deformation to microstructure in cortical bone using in situ loading, digital image correlation and synchrotron X-ray scattering. Acta Biomater. 69, 323–331.
Gustafsson, A., Wallin, M., Khayyeri, H., Isaksson, H., 2019b. Crack propagation in cortical bone is affected by the characteristics of the cement line: a parameter

study using an XFEM interface damage model. Biomech. Model. Mechanobiol., 1–15.
Hammond, M.A., Wallace, J.M., Allen, M.R., Siegmund, T., 2019. Mechanics of linear microcracking in trabecular bone. J. Biomech. 83, 34–42.
Hernandez, C.J., Keaveny, T.M., 2006. A biomechanical perspective on bone quality. Bone 39, 1173–1181.
Hui, S.L., Slemenda, C.W., Johnston Jr., C.C., 1988. Age and bone mass as predictors of fracture in a prospective study. J. Clin. Invest. 81, 1804–1809.
Idkaidek, A., Jasiuk, I., 2017. Cortical bone fracture analysis using XFEM - case study. Int. J. Numer. Method Biomed. Eng. 33.
Iori, G., Schneider, J., Reisinger, A., Heyer, F., Peralta, L., Wyers, C., Grasel, M., Barkmann, R., Gluer, C.C., van den Bergh, J.P., Pahr, D., Raum, K., 2019. Large cortical bone pores in the tibia are associated with proximal femur strength. PLoS ONE 14, e0215405.
Kanis, J.A., Cooper, C., Rizzoli, R., Reginster, J.Y., Scientific Advisory Board of the European Society for, C., Economic Aspects of, O., the Committees of Scientific, A., National Societies of the International Osteoporosis, F., 2019. European guidance for the diagnosis and management of osteoporosis in postmenopausal women. Osteoporos. Int. 30, 3–44.
Katsamenis, O.L., Jenkins, T., Thurner, P.J., 2015. Toughness and damage susceptibility in human cortical bone is proportional to mechanical inhomogeneity at the osteonal-level. Bone 76, 158–168.
Kennedy, O.D., Brennan, O., Mauer, P., Rackard, S.M., O'Brien, F.J., Taylor, D., Lee, T.C., 2008. The effects of increased intracortical remodeling on microcrack behaviour in compact bone. Bone 43, 889–893.
Koester, K.J., Ager 3rd, J.W., Ritchie, R.O., 2008. The true toughness of human cortical bone measured with realistically short cracks. Nat. Mater. 7, 672–677.
Koester, K.J., Barth, H.D., Ritchie, R.O., 2011. Effect of aging on the transverse toughness of human cortical bone: evaluation by R-curves. J. Mech. Behav. Biomed. Mater. 4, 1504–1513.
Li, S., Abdel-Wahab, A., Demirci, E., Silberschmidt, V.V., 2013. Fracture process in cortical bone: X-FEM analysis of microstructured models. Int. J. Fract. 184, 43–55.
Malo, M.K., Rohrbach, D., Isaksson, H., Toyras, J., Jurvelin, J.S., Tamminen, I.S., Kroger, H., Raum, K., 2013. Longitudinal elastic properties and porosity of cortical bone tissue vary with age in human proximal femur. Bone 53, 451–458.
Marco, M., Belda, R., Miguelez, M.H., Giner, E., 2018a. A heterogeneous orientation criterion for crack modelling in cortical bone using a phantom-node approach. Finite Elem. Anal. Des. 146, 107–117.
Marco, M., Giner, E., Larrainzar-Garijo, R., Caeiro, J.R., Miguelez, M.H., 2018b. Modelling of femur fracture using finite element procedures. Eng. Fract. Mech. 196, 157–167.
McCreadie, B.R., Goldstein, S.A., 2000. Biomechanics of fracture: is bone mineral density sufficient to assess risk? J. Bone Miner. Res. 15, 2305–2308.
Melton 3rd, L.J., 1990. A "Gompertzian" view of osteoporosis. Calcif. Tissue Int. 46, 285–286.
Milovanovic, P., vom Scheidt, A., Mletzko, K., Sarau, G., Püschel, K., Djuric, M., Amling, M., Christiansen, S., Busse, B., 2018. Bone tissue aging affects mineralization of cement lines. Bone 110, 187–193.
Mirzaali, M.J., Schwiedrzik, J.J., Thaiwichai, S., Best, J.P., Michler, J., Zysset, P.K., Wolfram, U., 2016. Mechanical properties of cortical bone and their relationships with age, gender, composition and microindentation properties in the elderly. Bone 93, 196–211.
Mischinski, S., Ural, A., 2011. Finite element modeling of microcrack growth in cortical bone. J. Appl. Mech. 78, 041016.
Nalla, R.K., Kruzic, J.J., Kinney, J.H., Balooch, M., Ager, J.W., Ritchie, R.O., 2006. Role of microstructure in the aging-related deterioration of the toughness of human cortical bone. Mater. Sci. Eng., C 26, 1251–1260.
Nalla, R.K., Kruzic, J.J., Kinney, J.H., Ritchie, R.O., 2004. Effect of aging on the toughness of human cortical bone: evaluation by R-curves. Bone 35, 1240–1246.
Nalla, R.K., Kruzic, J.J., Kinney, J.H., Ritchie, R.O., 2005. Mechanistic aspects of fracture and R-curve behavior in human cortical bone. Biomaterials 26, 217–231.
Nirody, J.A., Cheng, K.P., Parrish, R.M., Burghardt, A.J., Majumdar, S., Link, T.M., Kazakia, G.J., 2015. Spatial distribution of intracortical porosity varies across age and sex. Bone 75, 88–95.
Norman, T.L., Vashishth, D., Burr, D., 1995. Fracture toughness of human bone under tension. J. Biomech. 28, 313–320.
Obrien, F., Taylor, D., Clivelee, T., 2007. Bone as a composite material: The role of osteons as barriers to crack growth in compact bone. Int. J. Fatigue 29, 1051–1056.
Rho, J.Y., Zioupos, P., Currey, J.D., Pharr, G.M., 2002. Microstructural elasticity and regional heterogeneity in human femoral bone of various ages examined by nano-indentation. J. Biomech. 35, 189–198.
Ritchie, R.O., 2010. How does human bone resist fracture? Ann. NY Acad. Sci. 1192, 72–80.
Seref-Ferlengez, Zeynep, Kennedy, Oran D, Schaffler, Mitchell B, 2015. Bone microdamage, remodeling and bone fragility: how much damage is too much damage [quest]. BoneKEy reports 4. https://doi.org/10.1038/bonekey.2015.11.
Stein, M.S., Feik, S.A., Thomas, C.D., Clement, J.G., Wark, J.D., 1999. An automated analysis of intracortical porosity in human femoral bone across age. J. Bone Miner. Res. 14, 624–632.
Tong, X., Burton, I.S., Isaksson, H., Jurvelin, J.S., Kroger, H., 2015. Cortical bone histomorphometry in male femoral neck: the investigation of age-association and regional differences. Calcif. Tissue Int. 96, 295–306.
Unal, M., Creecy, A., Nyman, J.S., 2018. The role of matrix composition in the mechanical behavior of bone. Curr. Osteoporos. Rep. 16, 205–215.
Vergani, L., Colombo, C., Libonati, F., 2014. Crack propagation in cortical bone: A numerical study. Procedia Mater. Sci. 3, 1524–1529.
Wagermaier, W., Klaushofer, K., Fratzl, P., 2015. Fragility of Bone Material Controlled by Internal Interfaces. Calcif. Tissue Int. 97, 201–212.
Willett, T.L., Dapaah, D.Y., Uppuganti, S., Granke, M., Nyman, J.S., 2019. Bone collagen network integrity and transverse fracture toughness of human cortical bone. Bone 120, 187–193.
Zimmermann, E.A., Launey, M.E., Barth, H.D., Ritchie, R.O., 2009. Mixed-mode fracture of human cortical bone. Biomaterials 30, 5877–5884.
Zimmermann, E.A., Schaible, E., Bale, H., Barth, H.D., Tang, S.Y., Reichert, P., Busse, B., Alliston, T., Ager 3rd, J.W., Ritchie, R.O., 2011. Age-related changes in the plasticity and toughness of human cortical bone at multiple length scales. Proc. Natl. Acad. Sci. USA 108, 14416–14421.
Zimmermann, E.A., Schaible, E., Gludovatz, B., Schmidt, F.N., Riedel, C., Krause, M., Vettorazzi, E., Acevedo, C., Hahn, M., Puschel, K., Tang, S., Amling, M., Ritchie, R. O., Busse, B., 2016. Intrinsic mechanical behavior of femoral cortical bone in young, osteoporotic and bisphosphonate-treated individuals in low- and high energy fracture conditions. Sci. Rep. 6, 21072.
Zioupos, P., 2001. Accumulation of in-vivo fatigue microdamage and its relation to biomechanical properties in ageing human cortical bone. J. Microsc. 201, 270–278.